The Astrophysical Journal, 1000:76 (12pp), 2026 March 20 https://doi.org/10.3847/1538-4357/ae48fa

Bottom-up Formation of Phenol (C_6H_5OH) in Interstellar Analog Ices of Acetylene and Water Exposed to Ionizing Radiation

Jia Wang[1,2], Joshua H. Marks[1,2], Shiori Inada[1,2,3], and Ralf I. Kaiser[1,2]
[1] W. M. Keck Research Laboratory in Astrochemistry, University of Hawaii at Manoa, Honolulu, HI 96822, USA; ralfk@hawaii.edu
[2] Department of Chemistry, University of Hawaii at Manoa, Honolulu, HI 96822, USA
[3] Present address: Department of Basic Science, The University of Tokyo, 3-8-1 Komaba, Tokyo 153-8902, Japan
Received 2025 December 8; revised 2026 February 14; accepted 2026 February 21; published 2026 March 13

Abstract

Although oxygenated benzene derivatives are key precursors in the abiotic synthesis of biorelevant molecules and fundamental building blocks of functionalized polycyclic aromatic hydrocarbons, their formation mechanisms under interstellar conditions have remained largely unexplored. Here, we report the first bottom-up formation of phenol (C_6H_5OH) in low-temperature interstellar ice analogs composed of acetylene and water (C_2H_2–H_2O). Utilizing vacuum ultraviolet photoionization reflectron time-of-flight mass spectrometry and resonance-enhanced multiphoton ionization, phenol, along with aromatic hydrocarbons including benzene (C_6H_6), phenylacetylene (C_6H_5CCH), styrene ($C_6H_5CHCH_2$), naphthalene ($C_{10}H_8$), and phenanthrene ($C_{14}H_{10}$), were identified in the gas phase during temperature-programmed desorption. Among these species, styrene, naphthalene, and phenanthrene have not yet been detected in the interstellar medium, suggesting that they are suitable targets for future astronomical searches. These findings reveal viable low-temperature formation pathways for phenol through nonequilibrium chemistry in acetylene-containing interstellar ices, thereby advancing our understanding of the abiotic formation of oxygenated benzene derivatives in extraterrestrial environments.

Unified Astronomy Thesaurus concepts: Laboratory astrophysics (2004); Astrochemistry (75); Mass spectrometry (2094); Complex organic molecules (2256); Interstellar molecules (849)

1. Introduction

Since the first detection of benzene (C_6H_6) toward the protoplanetary nebula CRL 618 more than 20 yr ago (J. Cernicharo et al. 2001), benzene and its substituted derivatives have continued to attract considerable attention from the laboratory astrophysics (D. Nna-Mvondo & C. M. Anderson 2022; M. Tsuge et al. 2022; H. Abdoul-Carime et al. 2024; E. L. Piacentino et al. 2024), astrochemistry (B. A. McGuire et al. 2018; R. Ghosh et al. 2022; N. F. Kleimeier et al. 2022), theoretical chemistry (D. E. Woon & J.-Y. Park 2004; C. Xie et al. 2016; C. Robertson et al. 2021), and physical chemistry communities (N. Balucani et al. 1999; M. N. R. Ashfold et al. 2008; A. M. Thomas et al. 2019; R. I. Kaiser et al. 2022; D. Dey et al. 2024; S. J. Goettl et al. 2024). This broad interest mainly arises from their key roles as crucial precursors in the abiotic synthesis of biorelevant molecules linked to the origins of life (C. Menor-Salván et al. 2008; J. Wang et al. 2024a) and as fundamental molecular building blocks of polycyclic aromatic hydrocarbons (PAHs; S. J. Goettl et al. 2025). PAHs are ubiquitous in the interstellar medium (ISM) and are estimated to contain up to 30% of the total interstellar carbon (A. G. G. M. Tielens 2013; R. I. Kaiser et al. 2015; S. S. Zeichner et al. 2023; S. J. Goettl et al. 2025). PAHs such as indene (C_9H_8; A. M. Burkhardt et al. 2021; J. Cernicharo et al. 2021) and phenalene ($C_{13}H_{10}$; C. Cabezas et al. 2025), along with their cyanosubstituted derivatives with sizes extending up to cyanocoronene ($C_{24}H_{11}CN$; G. Wenzel et al. 2025), have been identified in the cold molecular cloud Taurus Molecular Cloud-1. These aromatic species may have been delivered to the early Earth via meteorites and comets (P. Ehrenfreund & J. Cami 2010). In fact, PAHs such as naphthalene ($C_{10}H_8$) and phenanthrene ($C_{14}H_{10}$), as well as benzene and oxygen- or nitrogen-substituted benzenes like phenol (C_6H_5OH) and benzonitrile (C_6H_5CN), have been identified in carbonaceous meteorites including Murchison and Winchcombe (S. Derenne & F. Robert 2010; J. S. Watson et al. 2010; A. Mojarro et al. 2023; M. A. Sephton et al. 2024). However, the formation mechanisms of PAHs and their substituted derivatives—particularly oxygenated PAHs (OPAHs)—under interstellar conditions have remained poorly understood (C. D. K. Herd et al. 2011; R. Ghosh et al. 2022; H. Abdoul-Carime et al. 2024).

As the simplest aromatic alcohols, phenol serves as a fundamental building block of OPAHs and represents a key molecular moiety in biologically relevant compounds, characterized by a hydroxyl (−OH) group directly bonded to an aromatic phenyl ring. Phenol has been tentatively detected toward the high-mass star-forming region Orion KL, with a column density of $(8 \pm 4) \times 10^{14}$ cm^{-2}, using the IRAM 30m line survey (L. Kolesniková et al. 2013). Additionally, an analysis of the band 4 Atacama Large Millimeter/submillimeter Array (ALMA) archival data for the hot molecular core G10.47+0.03 yielded an upper-limit column density of 7.0×10^{16} cm^{-2} for phenol (R. Ghosh et al. 2022). Through interactions with ultraviolet (UV) photons and galactic cosmic rays (GCRs), phenol can react with water (H_2O) to form benzenediols ($C_6H_4(OH)_2$) such as benzene-1,2-diol, benzene-1,3-diol, and benzene-1,4-diol (Figure 1). Subsequent oxidation of benzene-1,4-diol can yield benzoquinone ($C_6H_4O_2$), while benzene-1,2-diol may undergo reactions with interstellar ethylamine ($CH_3CH_2NH_2$; S. Zeng et al. 2021) and ethanolamine ($HOCH_2CH_2NH_2$; V. M. Rivilla et al. 2021), leading to the biorelevant neurotransmitters dopamine ($C_8H_{11}NO_2$) and norepinephrine ($C_8H_{11}NO_3$), respectively. Phenol may also

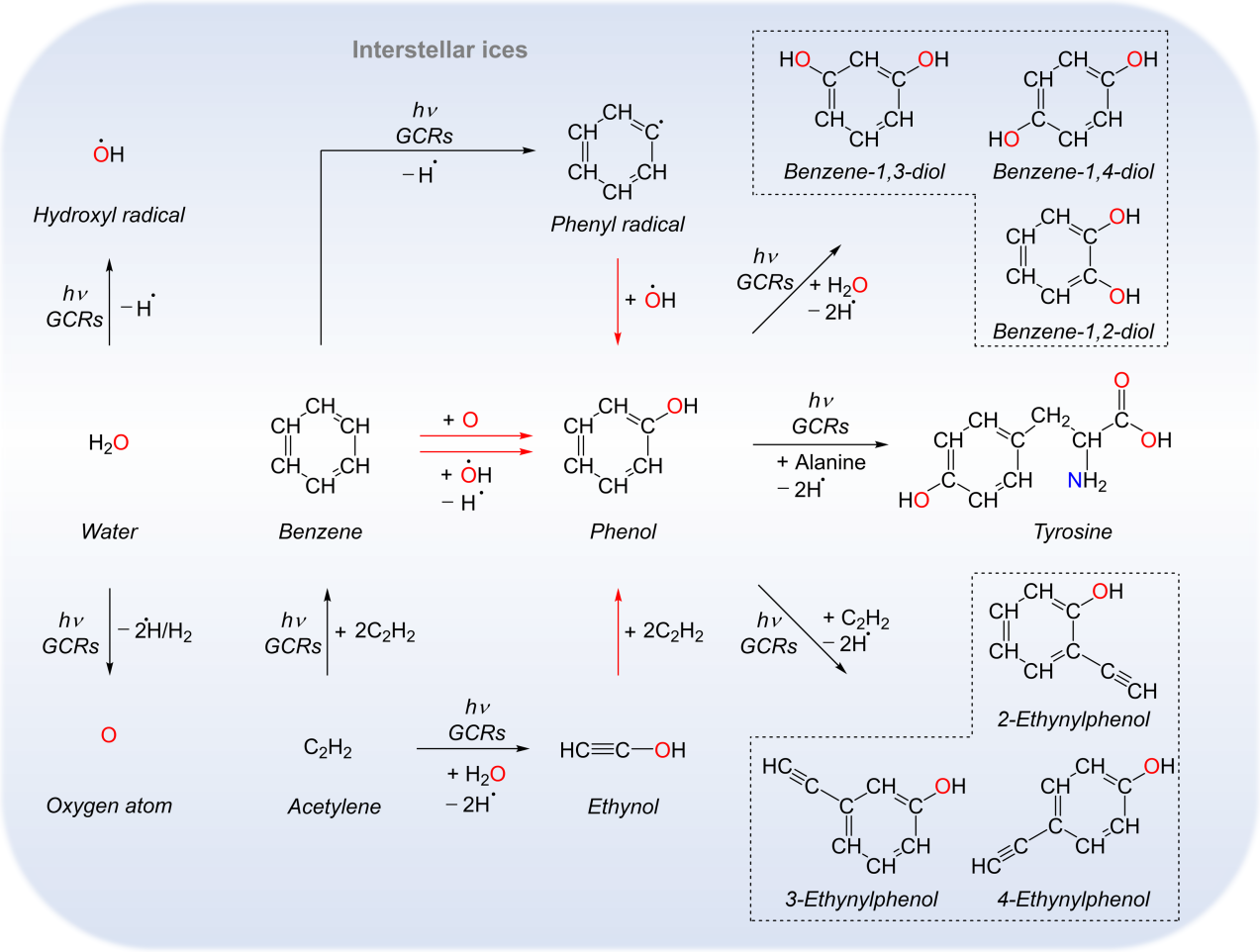

Figure 1. Proposed formation pathways of phenol in acetylene (C_2H_2)-rich and water (H_2O)-rich interstellar ices and its potential role as a precursor to complex aromatic compounds such as the amino acid tyrosine. Phenol may form through the reaction of benzene (C_6H_6) with either oxygen atom (O) or hydroxyl (OH) radical, the radical–radical recombination between the phenyl (C_6H_5) radical and the hydroxyl radical, or the reaction of ethynol (HCCOH) with two acetylene molecules (red arrows).

react with alanine ($NH_2CH(CH_3)COOH$) to form the essential amino acid tyrosine ($C_9H_{11}NO_3$), which plays a central role in the catalysis of enzymes such as photosystem II (B. A. Barry et al. 1990). Furthermore, the reaction of phenol with acetylene (C_2H_2) produces ethynylphenols ($C_6H_4(OH)CCH$), including 2-, 3-, and 4-ethynylphenol, which are key intermediates in the formation of OPAHs. Therefore, phenol could serve as a pivotal precursor to both OPAHs and biorelevant molecules in interstellar environments. A recent study on the benzonitrile–water ices irradiated by low-energy electrons (<10 eV) inferred the formation of phenol via quadrupole mass spectrometry (QMS) coupled with 70 eV electron impact ionization (H. Abdoul-Carime et al. 2024), but the interfering ion signals from structural isomers and the extensive fragmentation make an unambiguous identification of phenol impractical (A. M. Turner & R. I. Kaiser 2020). Hence, experimental evidence for the bottom-up formation of phenol under astrophysical conditions is still lacking.

Here, we present the first laboratory experiments on the bottom-up formation of phenol (C_6H_5OH) in low-temperature model interstellar ices composed of acetylene and water (C_2H_2–H_2O). Acetylene is ubiquitous in the ISM and has been detected in the gas phase in molecular clouds (J. H. Lacy et al. 1989), young stellar objects (YSOs; F. Lahuis & E. F. van Dishoeck 2000; J. S. Carr & J. R. Najita 2008), the carbon star IRC +10216 (S. T. Ridgway et al. 1976), and comets (M. J. Mumma et al. 2003). Solid-state acetylene has been detected on Titan (L. M. Lara et al. 1996) and has an estimated upper limit of 10% relative to water toward the massive YSO NGC7538:IRS9 (N. Boudin et al. 1998). Laboratory experiments have revealed that acetylene can form effectively in interstellar methane-containing ices via photolysis and radiolysis processes (R. I. Kaiser & K. Roessler 1998; B. M. Jones & R. I. Kaiser 2013; R. I. Kaiser et al. 2014; S. Maity et al. 2014; M. J. Abplanalp et al. 2018; N. F. Kleimeier & R. I. Kaiser 2022). Water is the most abundant constituent of interstellar ices (K. I. Öberg et al. 2011; A. G. G. M. Tielens 2013), with an abundance of over 50% of the interstellar ice observed in low-mass YSOs (A. C. A. Boogert et al. 2015). Therefore, acetylene−water ices serve as a suitable model system for investigating the bottom-up formation mechanisms of benzene and its substituted derivatives. The ice mixtures were irradiated at 5 K with energetic electrons, simulating the secondary electrons generated as GCRs penetrate interstellar ices in cold molecular clouds (B. C. Ferrari et al. 2021; R. Kaiser & K. Roessler 1997). The applied irradiation doses correspond to $(9 \pm 2) \times 10^6$ yr of GCR exposure in a cold molecular cloud (A. G. Yeghikyan 2011). Utilizing vacuum

ultraviolet (VUV) photoionization reflectron time-of-flight mass spectrometry (PI-ReToF-MS) combined with resonance-enhanced multiphoton ionization (REMPI), phenol (C_6H_5OH), benzene (C_6H_6), phenylacetylene (C_6H_5CCH), and styrene ($C_6H_5CHCH_2$), as well as PAHs including naphthalene ($C_{10}H_8$) and phenanthrene ($C_{14}H_{10}$), were identified in the gas phase isomer selectively during the temperature-programmed desorption (TPD) process. PI-ReToF-MS enables an isomer-specific identification using either single-photon ionization (PI; A. M. Turner & R. I. Kaiser 2020) or resonance-enhanced multiphoton ionization (REMPI; M. J. Abplanalp et al. 2019; N. F. Kleimeier et al. 2022; J. Wang et al. 2024a). PI-ReToF-MS distinguishes isomers based on their characteristic desorption profiles and adiabatic ionization energies (IEs). REMPI-ReToF-MS provides additional selectivity by resonantly exciting molecules to an isomer-specific electronic state prior to ionization, thereby offering higher sensitivity for aromatic species such as benzene and phenol and enabling the selective identification of isomers that cannot be differentiated by PI-ReToF-MS alone due to overlapping ionization energies. Our results suggest that phenol (C_6H_5OH), along with aromatics, can form in acetylene–water interstellar ices, highlighting that the previously astronomically undetected species styrene, naphthalene, and phenanthrene represent suitable targets for future gas-phase searches. Furthermore, these findings provide critical insights into the nonequilibrium formation pathways of phenol in interstellar ices, shedding light on the abiotic synthesis of OPAHs and their precursors in extraterrestrial environments.

2. Experiment

The experiments were conducted in a stainless steel ultrahigh vacuum chamber maintained at a base pressure of a few 10^{-11} Torr evacuated using magnetically levitated turbomolecular pumps (B. M. Jones & R. I. Kaiser 2013). Inside this chamber, a polished silver substrate was mounted on a cold head and cooled to 5 K using a two-stage closed-cycle helium cryostat (Sumitomo Heavy Industries, RDK-415E). The cold head was attached to a doubly differentially pumped rotatable flange, allowing free rotation, and can be translated vertically via an adjustable bellows (B. M. Jones & R. I. Kaiser 2013). Prior to deposition, the water (H_2O; HPLC, Fisher Scientific) sample was degassed in a borosilicate vial through multiple freeze–pump–thaw cycles using liquid nitrogen. After cooling the substrate to 5 K, the ices were prepared by simultaneously depositing acetylene (C_2H_2; 99.9%, Airgas) gas and water vapor through separate glass capillary arrays onto the substrate, maintaining an approximate partial-pressure ratio of 10:1 for C_2H_2 to H_2O. Although 5 K is slightly below the typical temperatures (10–15 K) of cold molecular clouds, this condition ensures that reactive intermediates remain intact and trapped, thereby providing valuable insights into the formation mechanisms of reaction products (J. Wang et al. 2024b). During the deposition, the ice thickness was monitored via laser interferometry using a helium-neon laser (CVI Melles-Griot, 25-LHP-230, 632.8 nm) directed at the substrate at a 4° incidence angle (A. M. Turner et al. 2015). Interference fringes in the reflected intensity, resulting from thin-film interference, were analyzed to monitor the ice growth. The refractive index of the mixed ice was taken as 1.31 ± 0.05, derived from reported refractive indexes of 1.34 for C_2H_2 ice at 10 K (R. L. Hudson et al. 2014) and 1.27 ± 0.02 for H_2O ice at 25 K (M. Bouilloud et al. 2015). The thickness of the ice mixture was determined to be 730 ± 50 nm. Fourier transform infrared (FTIR) spectra of the deposited ices were recorded between 6000 and 500 cm^{-1} at a spectral resolution of 1 cm^{-1} using a Thermo Electron Nicolet 6700 spectrometer. The ratio of C_2H_2 to H_2O was determined as (3.8 ± 1.0): 1 based on the integrated intensities of C_2H_2 bands at 3234 cm^{-1} (ν_3, 2.39×10^{-17} cm molecule^{-1}) and 747 cm^{-1} (ν_5, 2.42×10^{-17} cm molecule^{-1}) (R. L. Hudson et al. 2014), and of H_2O bands at 3381 cm^{-1} (ν_1, 1.7×10^{-16} cm molecule^{-1}; D. M. Hudgins et al. 1993) and 1608 cm^{-1} (ν_2, 9.0×10^{-18} cm molecule^{-1}; M. Bouilloud et al. 2015). Densities of 0.76 g cm^{-3} of C_2H_2 ice at 131 K (R. K. McMullan et al. 1992) and 0.87 ± 0.03 g cm^{-3} of H_2O ice at 25 K (M. Bouilloud et al. 2015) were used in these calculations.

The deposited ice mixtures were irradiated with 5 keV electrons at a current of 31 ± 1 nA for 45 minutes using an electron gun (SPECS, EQ PU-22). Monte Carlo simulations performed with the CASINO 2.42 software package (D. Drouin et al. 2007) were exploited to calculate the irradiation doses, yielding 2.0 ± 0.3 eV molecule^{-1} for C_2H_2 and 1.6 ± 0.3 eV molecule^{-1} for H_2O. These doses correspond to $(9 \pm 2) \times 10^6$ yr of GCR exposure in a cold molecular cloud (A. G. Yeghikyan 2011). The average electron penetration depth in the C_2H_2–H_2O ice was calculated to be 340 ± 50 nm, with 99% of the electron energy deposited within the upper 609 ± 50 nm of the ice mixture—well below the total ice thickness of 730 ± 50 nm—preventing interaction between the substrate and electrons. Infrared spectra of the ices were recorded in situ before, during, and after irradiation to monitor chemical evolution. Following irradiation, the ices were heated from 5 to 320 K at a rate of 0.5 K minute^{-1} for temperature-programmed desorption (TPD). During TPD, the subliming molecules were photoionized in the gas phase using pulsed (30 Hz) VUV light (10.49 eV; $3\omega_1$) or ultraviolet light (248, 266, and 275.15 nm; ω_2). To generate 10.49 eV photons, the third harmonic (355 nm) of an Nd:YAG laser (Spectra-Physics, Quanta Ray PRO 270–30) was frequency-tripled ($3\omega_1$) in a pulsed xenon gas (Specialty Gases, 99.999%) jet (J. Wang et al. 2023). The ultraviolet photons (ω_2) were produced by frequency doubling the output of a dye laser pumped by either the second (532 nm) or third harmonic (355 nm) of an Nd:YAG laser. Generation parameters for the VUV and ultraviolet photons are provided in Table A1. The selected VUV ($3\omega_1$) or UV (ω_2) beam was spatially separated from residual laser beams using a biconvex lithium fluoride lens (Korth Kristalle, $\phi = 38$ mm, $R_1 = R_2 = 131$ mm) in an off-axis configuration and was directed 2.0 ± 0.5 mm above the substrate to photoionize the subliming species during TPD. The resulting ions were mass-analyzed using a reflectron time-of-flight mass spectrometer (ReToF-MS; Jordan TOF Products, Inc.) and detected with a dual microchannel plate (MCP) detector. The MCP signals were amplified by a preamplifier (Ortec, 9305), then discriminated and further amplified to 4 V (Advanced Research Instruments Corp., F100-TD) before being recorded using a multichannel scaler (FAST ComTec, MCS6A). Each mass spectrum represented the sum of 3600 sweeps (2 minutes) with a temporal resolution of 3.2 ns. A blank experiment was also performed using C_2H_2–H_2O ice at 10.49 eV without electron irradiation.

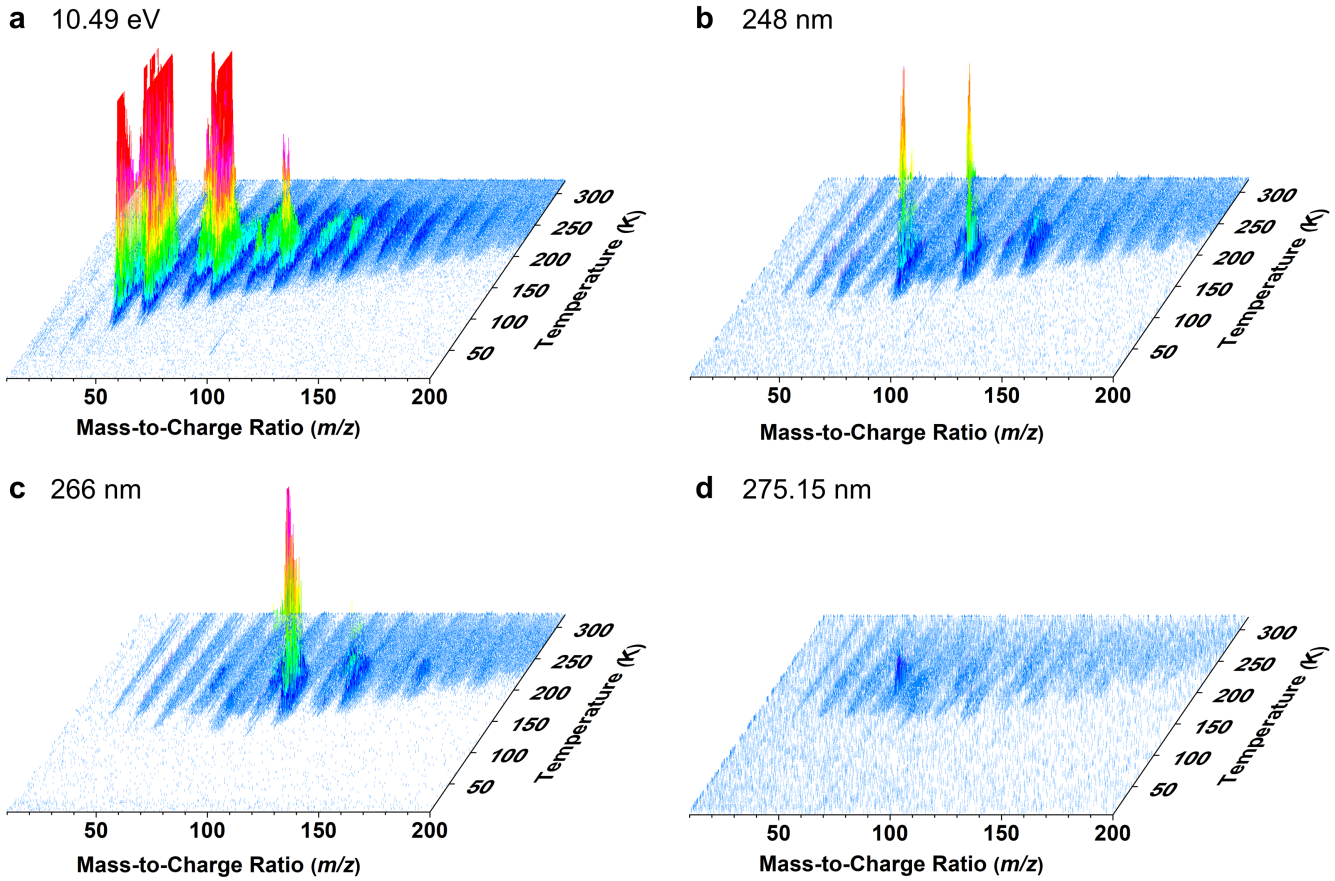

Figure 2. PI-ReToF-MS data of the irradiated C_2H_2–H_2O ices during TPD. Data were recorded at 10.49 eV (a), 248 nm (4.999 eV) (b), 266 nm (4.661 eV) (c), and 275.15 nm (4.506 eV) (d).

3. Results and Discussion

3.1. FTIR Analysis

FTIR spectra of acetylene–water (C_2H_2–H_2O) ices were recorded at 5 K before, during, and after electron irradiation (Figure A1 and Table A2). The absorptions of the unirradiated ices are dominated by characteristic vibrational modes of C_2H_2, such as the C–H stretching (ν_3, 3234 cm^{-1}) and C–H bending (ν_5, 747 cm^{-1}), and of H_2O, such as the O–H stretching (ν_1, 3381 cm^{-1}; ν_3, 3208 cm^{-1}). After irradiation, several weak absorption features appeared and were deconvolved using Gaussian functions. The C–H stretching (ν_4) mode of 1,3-butadiyne (C_4H_2) is observed at 3323 cm^{-1} (T. Koops et al. 1984). Absorptions at 3285 and 3093 cm^{-1} are assigned to the C–H stretching of vinylacetylene (ν_1, C_4H_4; Y. S. Kim & R. I. Kaiser 2009; E. Tørneng et al. 1980) and the CH_2 asymmetric stretching of ethylene (ν_9, C_2H_4; A. Brock et al. 1994), respectively. The absorption at 2974 cm^{-1} can be attributed to the combination (ν_6 + ν_7) of vinylacetylene (E. Tørneng et al. 1980; Y. S. Kim & R. I. Kaiser 2009), the CH_2 symmetric stretching (ν_{11}) of ethylene (A. Brock et al. 1994), and/or the CH_3 degenerate stretching (ν_{10}) of ethane (C_2H_6; J. J. Comeford & J. H. Gould 1961). The stretching vibration of carbon monoxide (CO) is detected at 2132 cm^{-1} (G. J. Jiang et al. 1975). However, due to the overlapping absorption features between phenol and water, the infrared absorptions of phenol cannot be distinguished under our experimental conditions, highlighting the need for a more sensitive analytical technique to identify individual complex reaction products.

3.2. PI-ReToF-MS and REMPI-ReToF-MS Analysis

The identification of phenol was achieved by PI-ReToF-MS and REMPI-ReToF-MS (A. M. Turner & R. I. Kaiser 2020). Figure 2 compiles PI-ReToF mass spectra of molecules subliming from the irradiated C_2H_2–H_2O ices, recorded at 10.49 eV, 248 nm (4.999 eV), 266 nm (4.661 eV), and 275.15 nm (4.506 eV). At a photon energy of 10.49 eV, the TPD profile of the ion signal at mass-to-charge (m/z) of 94 ($C_6H_6O^+$) exhibits two prominent desorption events peaking at 173 and 211 K, with desorption occurring from 136 to 320 K (Figure 3(a)). A blank experiment of the C_2H_2–H_2O ice was conducted at 10.49 eV under identical conditions but without electron irradiation; no obvious sublimation event was observed at $m/z = 94$, confirming that the ion signal at $m/z = 94$ arises from irradiation of the ices. At 10.49 eV, phenol (IE = 8.49 ± 0.02 eV; P. J. Linstrom & W. G. Mallard 2013) can be photoionized. However, multiple structural isomers with the same molecular formula C_6H_6O, such as benzene oxide and 2-ethenylfuran, can also be ionized at 10.49 eV; since their IE ranges overlap significantly, PI-ReToF-MS alone cannot unambiguously assign $m/z = 94$ signal to phenol, but only to a molecule of the formula C_6H_6O.

As mentioned above, REMPI-ReToF-MS provides a powerful approach to overcome the aforementioned limitations, allowing the identification of the species responsible for the ion signal at $m/z = 94$. Here, a one-color [1+1] REMPI scheme at 275.15 nm (4.506 eV) was employed to identify phenol. In this scheme, the first UV photon excites the phenol molecule to its $S_1 \leftarrow S_0$ origin band, followed by absorption of

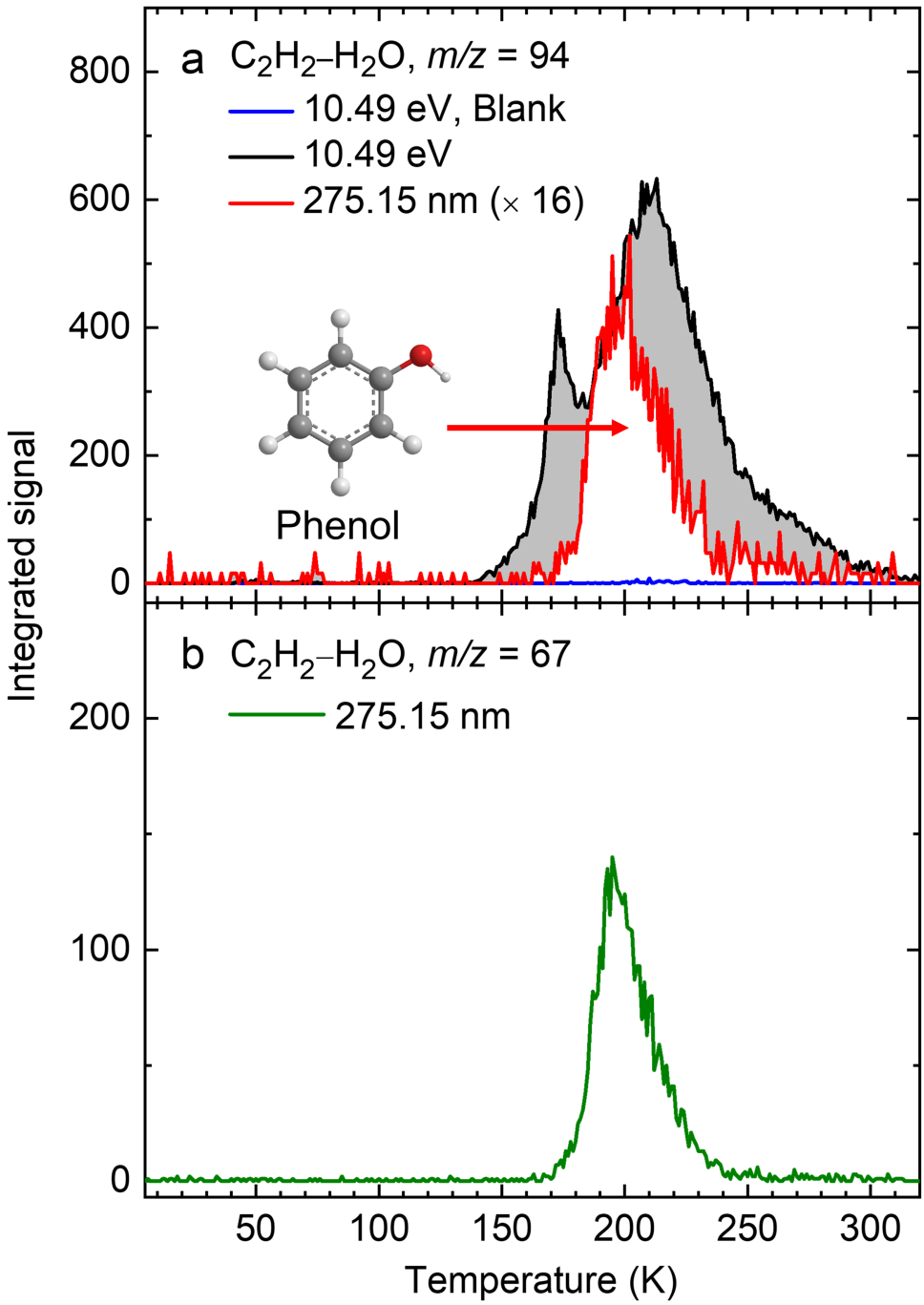

Figure 3. Ion signals of $m/z = 94$ and 67 during the TPD of C_2H_2–H_2O ices. (a) An overlay of single-photon ionization (10.49 eV) and [1 + 1] REMPI (275.15 nm) ion signals for phenol is shown as a function of temperature. The shaded region in gray indicates the desorption of structural isomers of phenol. (b) TPD profile of $m/z = 67$ from irradiated C_2H_2–H_2O ice recorded at 275.15 nm.

a second photon that ionizes the phenol molecule. Calibration gas-phase mass spectra of phenol were recorded at 296 K via [1 + 1] REMPI at 275.15 nm and VUV photoionization at 10.49 eV, both producing ion signals at $m/z = 94$ (Figures A2 (a) and (b)). Notably, the REMPI measurement at 275.15 nm reveals a strong ion signal observed at $m/z = 67$, which is assigned to the fragment $C_4H_3O^+$ from phenol. A separate experiment was performed with irradiated C_2H_2–H_2O ice to confirm the resonant REMPI wavelength of phenol based on the ion signals at $m/z = 67$ and 94. The resonance lines for phenol were determined at 275.0 ± 0.2 nm (Figures A2(c) and (d)) corresponding to its $S_1 \leftarrow S_0$ transition (H. D. Bist et al. 1967; C. Ratzer et al. 2002; M. G. D. Nix et al. 2006). The TPD profile of $m/z = 94$ obtained from the [1 + 1] REMPI measurement at 275.15 nm exhibits a sublimation event starting at 162 K and ending at 243 K (Figure 3(a)), providing evidence for the formation of phenol. This assignment is further supported by the concurrent detection of the ion signal at $m/z = 67$, whose TPD profile matches that of $m/z = 94$ (Figures 3(b) and A2(e)). An additional blank experiment of unirradiated phenol ice conducted under otherwise identical conditions at 10.49 eV shows the TPD profile of phenol at $m/z = 94$ spanning 159–251 K (Figure A2(f)), which is close to the sublimation temperatures observed at 275.15 nm

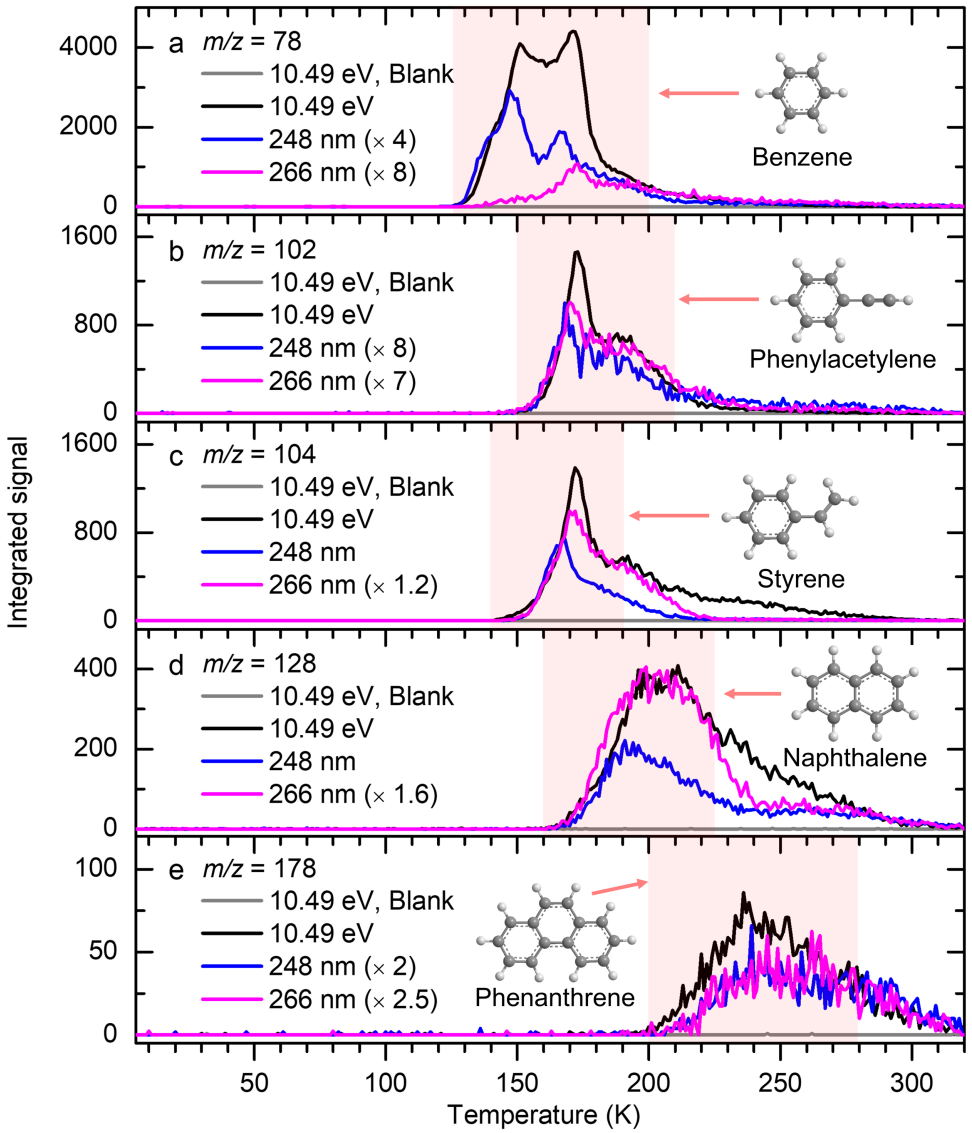

Figure 4. TPD profiles of $m/z = 78$ (a), $m/z = 102$ (b), $m/z = 104$ (c), $m/z = 128$ (d), and $m/z = 178$ (e) from C_2H_2–H_2O ices. Red shaded regions indicate the previously measured sublimation temperatures of benzene (a), phenylacetylene (b), styrene (c), naphthalene (d), and phenanthrene (e) from the irradiated C_2H_2 ices (M. J. Abplanalp et al. 2019).

(162–243 K), providing additional evidence for the phenol formation. A comparison of the TPD profiles of $m/z = 94$ obtained using PI- and REMPI-ReToF-MS reveals that phenol accounts for $(45 \pm 6)\%$ of the observed ion signal. The remaining signal must be attributed to other C_6H_6O isomers, which can be ionized via PI at 10.49 eV, but which cannot be ionized via the [1+1] REMPI scheme at 275.15 nm.

Besides the formation of phenol, the processed C_2H_2–H_2O ices also produce benzene (C_6H_6), phenylacetylene (C_6H_5CCH), styrene ($C_6H_5CHCH_2$), naphthalene ($C_{10}H_8$), and phenanthrene ($C_{14}H_{10}$), which contribute to the ion signals observed at $m/z = 78$, 102, 104, 128, and 178, respectively (Figure 4). At a photon energy of 10.49 eV, benzene (IE = 9.24378 ± 0.00007 eV), phenylacetylene (IE = 8.825 ± 0.001 eV), styrene (IE = 8.464 ± 0.001 eV), naphthalene (IE = 8.144 ± 0.001 eV), and phenanthrene (IE = 7.891 ± 0.001 eV) (J. M. Dyke et al. 1992; P. J. Linstrom & W. G. Mallard 2013) can be ionized. Since each molecular formula corresponds to multiple structural isomers, [1 + 1] REMPI measurements at 248 and 266 nm were performed, as these wavelengths are well suited for the detection of aromatic compounds (L. Cao et al. 2003; R. Hertz-Schünemann et al. 2013). Previous [1 + 1] REMPI studies at 248 and 266 nm have demonstrated the selective detection of benzene, styrene, naphthalene, and phenanthrene (H. J. Heger et al. 1999; L. Cao et al. 2003; A. Fendt et al. 2013; R. Hertz-Schünemann et al. 2013). The TPD profiles of $m/z = 78$, 102, 104, 128, and 178 recorded at these wavelengths indicate the formation of benzene, phenylacetylene, styrene, naphthalene, and phenanthrene, respectively. Furthermore, their sublimation temperature ranges are consistent with those previously reported for electron-irradiated C_2H_2 ices via [1 + 1] REMPI detection of the subliming molecules in the TPD phase (M. J. Abplanalp et al. 2019; N. F. Kleimeier et al. 2022). Note that the relatively weak ion signal of benzene ($m/z = 78$) at 266 nm results from its low ionization efficiency at this wavelength (L. Cao et al. 2003). Additional TPD profiles of $m/z = 110$, 118, 120, 144, and 194 were also observed during TPD of irradiated C_2H_2–H_2O ices at 248 and 266 nm (Figure A3 and Table A3). These signals may be associated with benzenediols ($C_6H_4(OH)_2$; W. L. Holstein et al. 2001; A. Fendt et al. 2013;

R. Hertz-Schünemann et al. 2013), ethynylphenols ($C_6H_4(OH)CCH$), ethenylphenols ($C_6H_4(OH)CHCH_2$; A. Fendt et al. 2013), naphthols ($C_{10}H_8O$), and anthrols ($C_{14}H_{10}O$), respectively.

3.3. Formation Pathways

The above PI- and REMPI-ReToF-MS measurements demonstrate the gas-phase detection of phenol and aromatic hydrocarbons, including benzene, phenylacetylene, styrene, naphthalene, and phenanthrene, during TPD of irradiated C_2H_2–H_2O ices. We now turn to their potential formation pathways in irradiated model interstellar ices composed of acetylene and water. The formation routes of benzene and PAHs such as naphthalene and phenanthrene in processed C_2H_2 ices have already been discussed in previous studies (M. J. Abplanalp et al. 2019; M. J. Abplanalp & R. I. Kaiser 2020; N. F. Kleimeier et al. 2022); therefore, we focus here only on the potential formation pathways leading to phenol. Upon interaction with energetic electrons, water can undergo unimolecular decomposition via Reaction (1), producing a hydroxyl radical (OH) and a hydrogen atom (H) (W. Zheng et al. 2006) or via Reaction (2), yielding an oxygen atom (O) plus two hydrogen atoms or molecular hydrogen (H_2). Since Reactions (1) and (2) are strongly endoergic, energy deposition from GCR-generated secondary electrons is required to initiate these pathways. Once formed, the oxygen atom or hydroxyl radical can react with benzene to produce phenol via Reaction (3) through insertion into a carbon–hydrogen bond and Reaction (4) via hydroxyl radical addition to the aromatic system followed by atomic hydrogen elimination (J. K. Parker & S. R. Davis 1999; T. Seta et al. 2006; R. Ghosh et al. 2022), with reaction energies of −422 and +4 kJ mol^{-1}, respectively (B. Ruscic and H. Bross, 2025). Alternatively, benzene can undergo C–H bond cleavage to yield a phenyl radical (C_6H_5) and a hydrogen atom via Reaction (5) (S. J. Goettl et al. 2025). The resulting phenyl radical may then recombine barrierlessly with a nearby hydroxyl radical—provided a favorable geometry—to form phenol even at 5 K through Reaction (6) (R. Ghosh et al. 2022). Reaction (6) is exoergic by 464 kJ mol^{-1} (B. Ruscic & H. Bross 2025). Finally, the formation of phenol may proceed through ethynol (HCCOH), which can form via the radical–radical recombination of the ethynyl (C_2H) and hydroxyl (OH) radicals (A. M. Turner et al. 2020). Ethynol can subsequently react with two acetylene molecules to phenol via Reaction (7), an exoergic process with a reaction energy of 627 kJ mol^{-1} (B. Ruscic & H. Bross 2025). This pathway is similar to the formation of benzene in acetylene ices exposed to ionizing radiation (J. Wang et al. 2024a; L. Zhou et al. 2010).

$$H_2O \rightarrow OH + H, \quad \Delta H_r^\circ(0\,K) = +492\ \text{kJ mol}^{-1}, \tag{1}$$

$$H_2O \rightarrow O + 2H/H_2, \quad \Delta H_r^\circ(0\,K) = +918/+486\ \text{kJ mol}^{-1}, \tag{2}$$

$$C_6H_6 + O \rightarrow C_6H_5OH, \quad \Delta H_r^\circ(0\,K) = -422\ \text{kJ mol}^{-1}, \tag{3}$$

$$C_6H_6 + OH \rightarrow C_6H_5OH + H, \quad \Delta H_r^\circ(0\,K) = +4\ \text{kJ mol}^{-1}, \tag{4}$$

$$C_6H_6 \rightarrow C_6H_5 + H, \quad \Delta H_r^\circ(0\,K) = +468\ \text{kJ mol}^{-1}, \tag{5}$$

$$C_6H_5 + OH \rightarrow C_6H_5OH, \quad \Delta H_r^\circ(0\,K) = -464\ \text{kJ mol}^{-1}, \tag{6}$$

$$HCCOH + 2C_2H_2 \rightarrow C_6H_5OH, \quad \Delta H_r^\circ(0\,K) = -627\ \text{kJ mol}^{-1}. \tag{7}$$

4. Astrophysical Implications and Conclusions

This study presents the first laboratory experiments on the bottom-up formation of phenol (C_6H_5OH) in low-temperature model interstellar acetylene–water (C_2H_2–H_2O) ices. The ice mixtures were irradiated with energetic electrons as GCR proxies, with irradiation doses of 2.0 ± 0.3 eV molecule^{-1} for C_2H_2 and 1.6 ± 0.3 eV molecule^{-1} for H_2O. These doses are equivalent to GCR exposure in interstellar ices within a cold molecular cloud aged up to 9×10^6 yr, corresponding to its early evolutionary stage (A. G. Yeghikyan 2011). Utilizing PI- and REMPI-ReToF-MS, phenol, along with aromatic hydrocarbons including benzene, phenylacetylene, styrene, naphthalene, and phenanthrene, were detected in the gas phase during TPD, simulating the thermal desorption that occurs as a cold molecular cloud evolves toward star formation. Based on gas-phase identification of these compounds during TPD, our results suggest that low-temperature formation pathways to phenol in acetylene-rich ices are feasible and provide valuable constraints for astrochemical models of its formation in the ISM. It is worth noting that the formation of phenol via radical–radical recombination can proceed either at low temperatures of 5 K during irradiation or at higher temperatures during TPD. At low temperatures, radicals can recombine without diffusion if a favorable geometry is present, whereas others may be preserved in the ice due to limited mobility. As the matrix warms during TPD, diffusive mechanisms may compete with nondiffusive pathways at higher temperatures. However, the present experiments cannot distinguish between these formation mechanisms. Once formed, phenol may react with water and acetylene to produce benzenediols and ethynylphenols, respectively (Figure 1), contributing to the synthesis of oxygenated PAHs (OPAHs). Although benzene, phenylacetylene, styrene, naphthalene, and phenanthrene have previously been identified in processed acetylene ices (M. J. Abplanalp et al. 2019; N. F. Kleimeier et al. 2022; C. Zhang et al. 2023), we present their first detection in interstellar ice analogs by incorporating water—the most abundant constituent of interstellar ices (K. I. Öberg et al. 2011; A. G. G. M. Tielens 2013).

Acetylene is widespread in astrophysical environments (S. T. Ridgway et al. 1976; J. H. Lacy et al. 1989; L. M. Lara et al. 1996; N. Boudin et al. 1998; F. Lahuis & E. F. van Dishoeck 2000; A. M. S. Boonman et al. 2003) and can be synthesized in methane-containing interstellar ices through radiation processing (R. I. Kaiser & K. Roessler 1998; B. M. Jones & R. I. Kaiser 2013; R. I. Kaiser et al. 2014; S. Maity et al. 2014; M. J. Abplanalp et al. 2018; N. F. Kleimeier & R. I. Kaiser 2022), making acetylene–water ice an suitable model system for studying the formation of substituted benzene derivatives such as phenol. Our results suggest that phenol and the detected aromatic hydrocarbons can likely form in these interstellar environments. Once formed, these compounds can desorb into the gas phase as molecular clouds undergo the transition to hot cores at temperatures exceeding some 180 K and thus represent suitable targets for gas-phase searches via telescopes such as ALMA. In fact, using the IRAM 30m line survey, L. Kolesniková et al. (2013) tentatively detected phenol toward Orion KL with a column density of $(8 \pm 4) \times 10^{14}$ cm^{-2} (L. Kolesniková et al. 2013). A

subsequent analysis of the band 4 ALMA archival data for the hot molecular core G10.47+0.03 provided an upper limit of 7.0×10^{16} cm^{-2} for phenol (R. Ghosh et al. 2022). Given that acetylene has also been detected toward Orion-KL with abundances up to 4.9×10^{-7} relative to molecular hydrogen (A. M. S. Boonman et al. 2003), our results offer a mechanistic explanation for phenol formation in regions such as Orion KL. Although the ratio of acetylene to water used in the experiments is not a typical abundance ratio estimated for cometary (N. Biver et al. 2024; B. P. Bonev et al. 2023) and interstellar ices (F. Lahuis & E. F. van Dishoeck 2000), this ratio ensures the highest possible yield of products such as benzene and phenol, and thus facilitates their detection. Future experiments can be conducted by varying the acetylene-to-water ratio toward more realistic values of ~0.1%–0.5% (F. Lahuis & E. F. van Dishoeck 2000) to investigate the effects of dilution.

Acknowledgments

This work was supported by the U.S. National Science Foundation (NSF), Division of Astronomical Sciences (AST-2403867), awarded to the University of Hawaii at Manoa.

Appendix

The generation parameters of vacuum ultraviolet photons are summarized in Table A1. The FTIR spectra of acetylene–water ices recorded before and after irradiation, together with their absorption assignments, are shown in Figure A1 and Table A2. The mass spectra of phenol, TPD profiles, and additional tentative molecular formula assignments of products formed from irradiated acetylene–water are presented in Figures A2–A3 and Table A3.

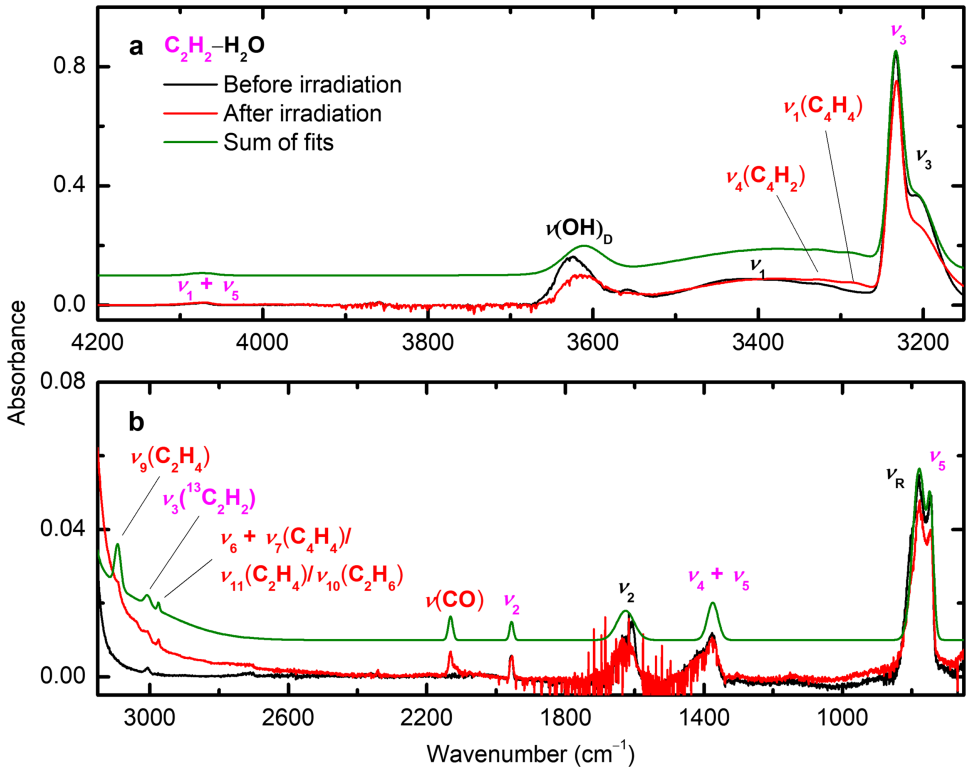

Figure A1. Baseline-corrected infrared spectra of C_2H_2–H_2O ice before (black) and after (red) irradiation with deconvolution of the regions: 4200–3150 cm^{-1} (a) and 3150–650 cm^{-1} (b). The green lines represent the total fit to the spectra and are offset by 0.1 in (a) and 0.01 in (b) for clarity. Detailed assignments are provided in Table A2.

Table A1
Generation Parameters of Vacuum Ultraviolet (VUV; $3\omega_1$) and Ultraviolet (UV; ω_2) Photons

Photon Energy (eV)	10.49 ($3\omega_1$)	4.999 (ω_2)	4.661 (ω_2)	4.506 (ω_2)
Nonlinear medium for four-wave mixing	Xenon	…	…	…
ω_1 wavelength (nm)	355	…	…	…
Nd:YAG 1 output (nm)	355	…	…	…
ω_2 wavelength (nm) [a]	…	248	266	275.15
Nd:YAG 2 output (nm)	…	355	355	532
Dye laser output (nm)	…	496	532	550.30
ω_2 Dye	…	Coumarin 503	Coumarin 540A	Pyrromethene 580

Note.
[a] obtained via frequency doubling process.

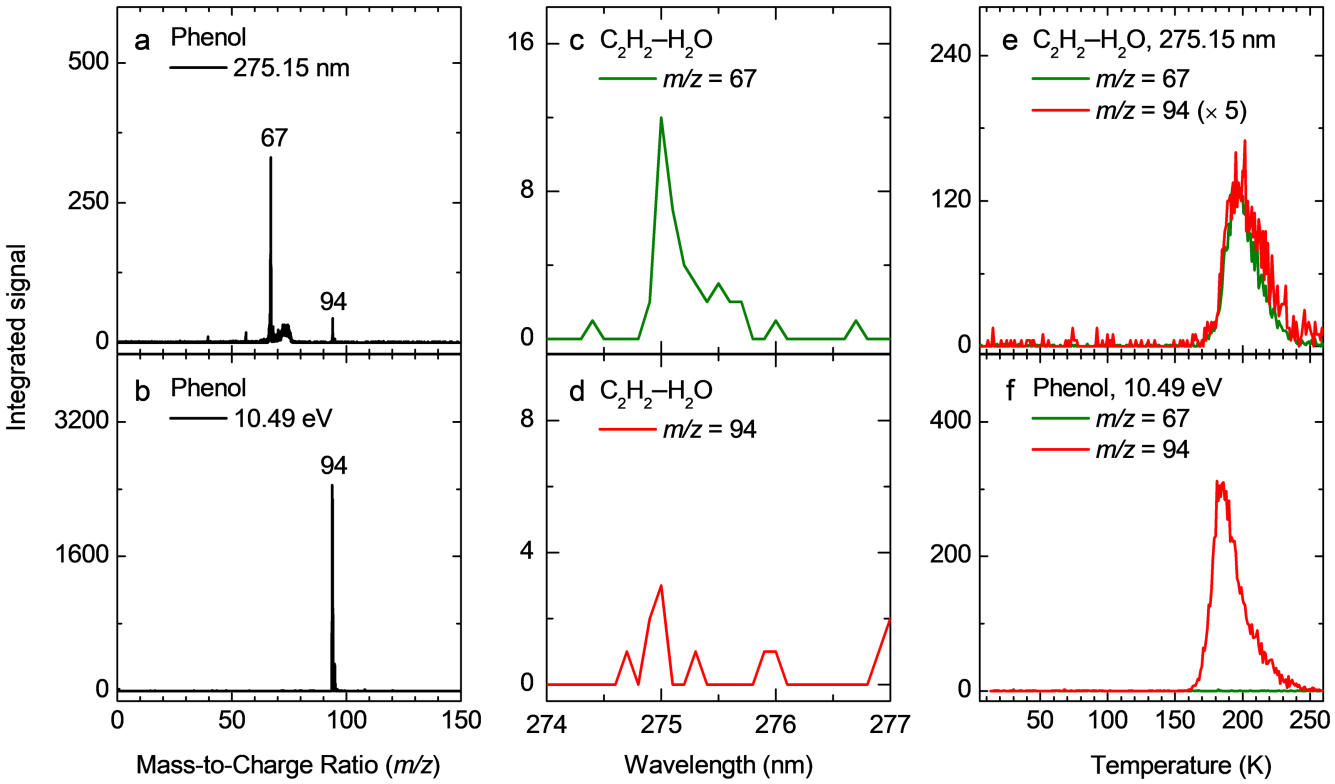

Figure A2. Gas-phase mass spectra of phenol (C_5H_6OH, $m/z = 94$) recorded at 296 K using [1 + 1] REMPI at 275.15 nm (a) and VUV photoionization at 10.49 eV (b). REMPI scans (274–277 nm) for $m/z = 67$ (c) and 94 (d) collected from the irradiated C_2H_2–H_2O ice during sublimation temperatures between 189 and 210 K. TPD profiles of $m/z = 67$ and 94 from irradiated C_2H_2–H_2O ice recorded at 275.15 nm (e) and the unirradiated phenol ice recorded at 10.49 eV (f).

Table A2
IR Absorptions Observed in C_2H_2–H_2O Ice before and after Electron Irradiation (30 nA, 45 Minutes) at 5 K

Pristine Ice, Absorptions before Irradiation (cm^{-1})	Assignment
C_2H_2	Assignment (G. L. Bottger & D. F. Eggers 1964; R. L. Hudson et al. 2014; K. D. Doney et al. 2018)
4074	$\nu_1 + \nu_5$
3234	ν_3
3004	$\nu_3(^{13}C_2H_2)$
1955	ν_2
1375	$\nu_4 + \nu_5$
747	ν_5
H_2O	Assignment (W. Hagen et al. 1981; L. B. D'Hendecourt & L. J. Allamandola 1986)
3625	$\nu(OH)_D$
3381	ν_1
3208	ν_3
1608	ν_2
777	ν_R
New absorptions after irradiation (cm^{-1})	Assignment
3323	$\nu_4(C_4H_2)$ (T. Koops et al. 1984)
3285	$\nu_1(C_4H_4)$ (E. Tørneng et al. 1980)
3093	$\nu_9(C_2H_4)$ (A. Brock et al. 1994)
2975	$\nu_6+\nu_7(C_4H_4)/\nu_{11}(C_2H_4)/\nu_{10}(C_2H_6)$ (J. J. Comeford & J. H. Gould 1961; E. Tørneng et al. 1980; A. Brock et al. 1994)
2132	ν(CO) (G. J. Jiang et al. 1975)

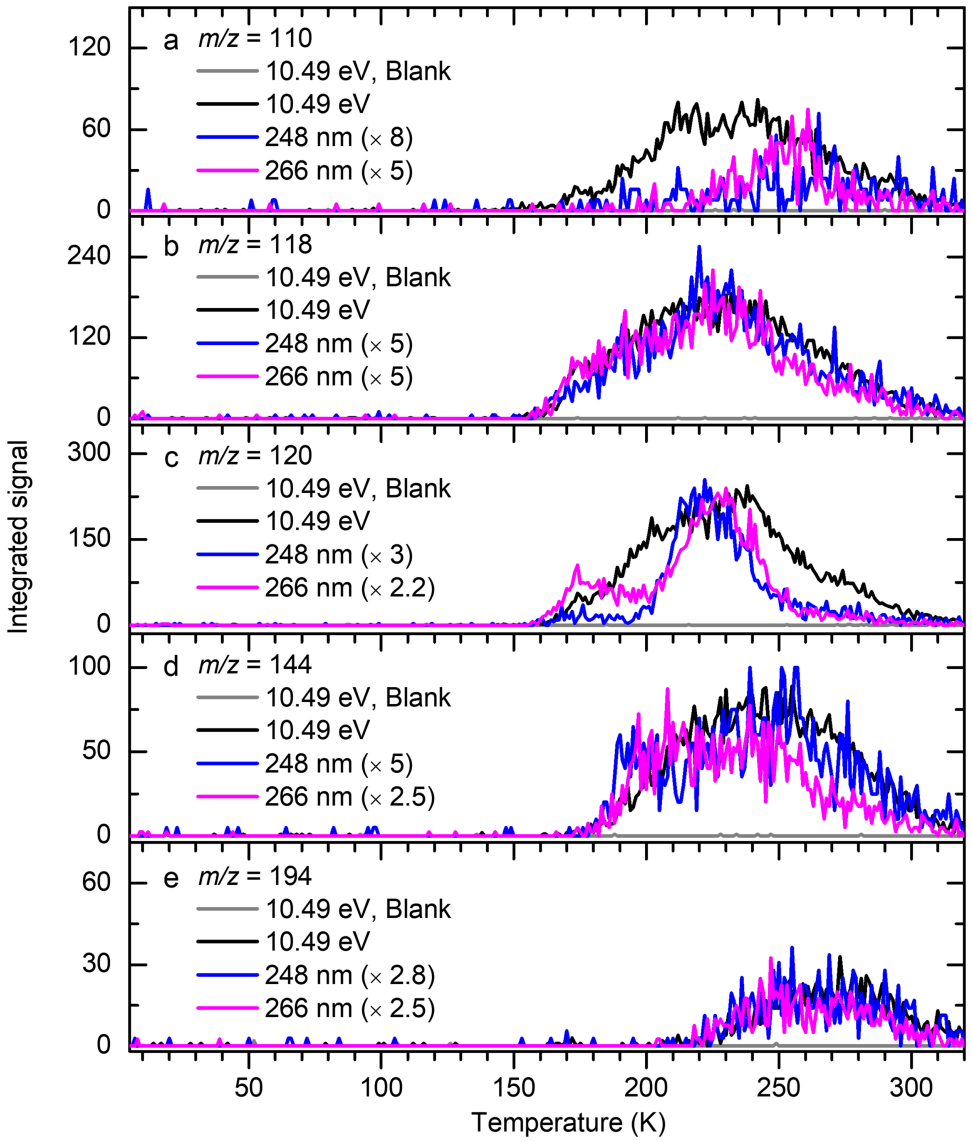

Figure A3. TPD profiles of $m/z = 110$ (a), $m/z = 118$ (b), $m/z = 120$ (c), $m/z = 144$ (d), and $m/z = 194$ (e) from C_2H_2–H_2O ices.

Table A3
Observed Mass-to-charge Ratios (*m/z*) from Irradiated C_2H_2–H_2O Ice Recorded at 10.49 eV and Their Tentative Molecular Formula Assignments Based on Previously Measured Irradiated C_2H_2 Ices (M. J. Abplanalp & R. I. Kaiser 2020)

m/z	Possible Molecular Formula(e)	*m/z*	Possible Molecular Formula(e)
28	C_2H_4	136	$C_{10}H_{16}$, $C_{11}H_4$, $C_9H_{12}O$, $C_8H_8O_2$
40	C_3H_4	138	$C_{10}H_{18}$, $C_{11}H_6$, $C_{10}H_2O$, $C_8H_{10}O_2$
42	C_3H_6, C_2H_2O	140	$C_{10}H_{20}$, $C_{11}H_8$, $C_{10}H_4O$, $C_8H_{12}O_2$
44	C_2H_4O	142	$C_{10}H_{22}$, $C_{11}H_{10}$, $C_{10}H_6O$, $C_8H_{14}O_2$
50	C_4H_2	144	$C_{11}H_{12}$, $C_{10}H_8O$, $C_8H_{16}O_2$
52	C_4H_4	146	$C_{11}H_{14}$, $C_{12}H_2$, $C_{10}H_{10}O$
54	C_4H_6, C_3H_2O	148	$C_{11}H_{16}$, $C_{12}H_4$, $C_{10}H_{12}O$
56	C_4H_8, C_3H_4O	150	$C_{11}H_{18}$, $C_{12}H_6$, $C_{10}H_{14}O$
58	C_4H_{10}, C_3H_6O, $C_2H_2O_2$	152	$C_{11}H_{20}$, $C_{12}H_8$, $C_{10}H_{16}O$
60	C_3H_8O, $C_2H_4O_2$	154	$C_{11}H_{22}$, $C_{12}H_{10}$, $C_{10}H_{18}O$, $C_{10}H_2O_2$
64	C_5H_4	156	$C_{11}H_{24}$, $C_{12}H_{12}$, $C_{10}H_{20}O$, $C_{10}H_4O_2$
66	C_5H_6, C_4H_2O	158	$C_{13}H_2$, $C_{12}H_{14}$, $C_{10}H_{22}O$, $C_{10}H_6O_2$
68	C_5H_8, C_4H_4O	160	$C_{13}H_4$, $C_{12}H_{16}$, $C_{10}H_{24}O$, $C_{10}H_8O_2$
70	C_5H_{10}, C_4H_6O, $C_3H_2O_2$	162	$C_{12}H_{18}$, $C_{11}H_{14}O$, $C_{12}H_2O$, $C_{10}H_{10}O_2$
72	C_5H_{12}, C_4H_8O, $C_3H_4O_2$	164	$C_{12}H_{20}$, $C_{11}H_{16}O$, $C_{12}H_4O$, $C_{10}H_{12}O_2$
74	C_6H_2, $C_4H_{10}O$, $C_3H_6O_2$	166	$C_{12}H_{22}$, $C_{11}H_{18}O$, $C_{12}H_6O$, $C_{10}H_{14}O_2$
76	C_6H_4, $C_4H_{12}O$, $C_3H_8O_2$	168	$C_{12}H_{24}$, $C_{11}H_{20}O$, $C_{12}H_8O$, $C_{10}H_{16}O_2$
78	C_6H_4, C_5H_2O	170	$C_{13}H_{14}$, $C_{12}H_{26}$, $C_{12}H_{10}O$, $C_{10}H_{18}O_2$
80	C_6H_8, C_5H_4O	176	$C_{13}H_{20}$, $C_{14}H_8$, $C_{12}H_{16}O$
82	C_6H_{10}, C_5H_6O, $C_4H_2O_2$	178	$C_{13}H_{22}$, $C_{14}H_{10}$, $C_{12}H_{18}O$, $C_{12}H_2O_2$
84	C_6H_{12}, C_5H_8O, $C_4H_4O_2$	180	$C_{13}H_{24}$, $C_{14}H_{12}$, $C_{12}H_{20}O$, $C_{12}H_4O_2$
86	C_7H_2, C_6H_{14}, $C_5H_{10}O$	182	$C_{13}H_{26}$, $C_{14}H_{14}$, $C_{12}H_{22}O$, $C_{12}H_6O_2$
88	C_7H_4, $C_5H_{12}O$, $C_4H_8O_2$	184	$C_{13}H_{28}$, $C_{14}H_{16}$, $C_{12}H_{24}O$, $C_{12}H_8O_2$
90	C_7H_6, C_6H_2O, $C_4H_{10}O_2$	186	$C_{14}H_{18}$, $C_{14}H_2O$, $C_{12}H_{26}O$, $C_{12}H_{10}O_2$
92	C_7H_8, C_6H_4O	188	$C_{14}H_{20}$, $C_{14}H_4O$, $C_{12}H_{12}O_2$
94	C_7H_{10}, C_6H_6O	190	$C_{14}H_{22}$, $C_{14}H_6O$, $C_{12}H_{14}O_2$
96	C_7H_{12}, C_6H_8O	192	$C_{14}H_{24}$, $C_{14}H_8O$, $C_{12}H_{16}O_2$
98	C_8H_2, C_7H_{14}, $C_6H_{10}O$	194	$C_{15}H_{14}$, $C_{14}H_{26}$, $C_{14}H_{10}O$, $C_{12}H_{18}O_2$
102	C_8H_6, C_7H_2O, $C_6H_{14}O$	196	$C_{14}H_{28}$, $C_{15}H_{16}$ $C_{14}H_{12}O$, $C_{12}H_{20}O_2$
104	C_8H_8, C_7H_4O, $C_5H_{12}O_2$	198	$C_{14}H_{30}$, $C_{14}H_{14}O$, $C_{12}H_{22}O_2$
106	C_8H_{10}, C_7H_6O, $C_6H_2O_2$	200	$C_{15}H_{20}$, $C_{14}H_{16}O$, $C_{12}H_{24}O_2$
108	C_8H_{12}, C_7H_8O, $C_6H_4O_2$	202	$C_{15}H_{22}$, $C_{14}H_{18}O$, $C_{15}H_6O$
110	C_9H_2, C_8H_{14}, $C_7H_{10}O$, $C_6H_6O_2$	204	$C_{15}H_{24}$, $C_{14}H_{20}O$, $C_{15}H_8O$
112	C_9H_4, C_8H_{16}, $C_7H_{12}O$, $C_6H_8O_2$	208	$C_{16}H_{14}$, $C_{14}H_{24}O$, $C_{15}H_{12}O$
114	C_9H_6, C_8H_{18}, $C_7H_{14}O$, $C_6H_{10}O_2$	210	$C_{16}H_{16}$, $C_{14}H_{26}O$, $C_{15}H_{14}O$
116	C_9H_8, $C_7H_{16}O$, C_8H_4O, $C_6H_{12}O_2$	212	$C_{15}H_{32}$, $C_{14}H_{28}O$, $C_{15}H_{16}O$
118	C_9H_{10}, C_8H_6O, $C_6H_{14}O_2$	214	$C_{16}H_{22}$, $C_{14}H_{30}O$, $C_{15}H_{18}O$
120	C_9H_{12}, C_8H_8O	216	$C_{16}H_{24}$, $C_{15}H_{20}O$, $C_{16}H_8O$
122	C_9H_{14}, $C_{10}H_2$, $C_8H_{10}O$	218	$C_{16}H_{26}$, $C_{15}H_{22}O$, $C_{16}H_{10}O$
124	C_9H_{16}, $C_{10}H_4$, $C_8H_{12}O$	224	$C_{16}H_{32}$, $C_{15}H_{28}O$, $C_{16}H_{16}O$
126	C_9H_{18}, $C_{10}H_6$, $C_8H_{14}O$, C_9H_2O	226	$C_{16}H_{34}$, $C_{15}H_{30}O$, $C_{16}H_{18}O$
128	C_9H_{20}, $C_{10}H_8$, $C_8H_{16}O$, C_9H_4O	228	$C_{17}H_{24}$, $C_{16}H_{20}O$, $C_{17}H_8O$
130	$C_{10}H_{10}$, $C_8H_{18}O$, C_9H_6O, $C_8H_2O_2$	230	$C_{17}H_{26}$, $C_{16}H_{22}O$, $C_{17}H_{10}O$
132	$C_{10}H_{12}$, C_9H_8O, $C_7H_{16}O_2$, $C_8H_4O_2$	256	$C_{20}H_{16}$, $C_{18}H_{24}O$, $C_{19}H_{12}O$
134	$C_{10}H_{14}$, $C_{11}H_2$, $C_9H_{10}O$, $C_8H_6O_2$	284	$C_{22}H_{20}$, $C_{20}H_{28}O$, $C_{21}H_{16}O$

ORCID iDs

Jia Wang https://orcid.org/0000-0002-3795-8699
Joshua H. Marks https://orcid.org/0000-0003-0492-2494
Ralf I. Kaiser https://orcid.org/0000-0002-7233-7206

References

Abdoul-Carime, H., Lathuilière, B., Nedelec, P., & Kopyra, J. 2024, JGRE, 129, e2023JE008151
Abplanalp, M. J., Frigge, R., & Kaiser, R. I. 2019, SciA, 5, eaaw5841
Abplanalp, M. J., Jones, B. M., & Kaiser, R. I. 2018, PCCP, 20, 5435
Abplanalp, M. J., & Kaiser, R. I. 2020, ApJ, 889, 3
Ashfold, M. N. R., Devine, A. L., Dixon, R. N., et al. 2008, PNAS, 105, 12701
Balucani, N., Asvany, O., Chang, A. H. H., et al. 1999, JChPh, 111, 7457
Barry, B. A., el-Deeb, M. K., Sandusky, P. O., & Babcock, G. T. 1990, JBiCh, 265, 20139
Bist, H. D., Brand, J. C. D., & Williams, D. R. 1967, JMoSp, 24, 413
Biver, N., Bockelée-Morvan, D., Handzlik, B., et al. 2024, A&A, 690, A271
Bonev, B. P., Dello Russo, N., Kawakita, H., et al. 2023, AJ, 166, 233
Boogert, A. C. A., Gerakines, P. A., & Whittet, D. C. B. 2015, ARA&A, 53, 541
Boonman, A. M. S., van Dishoeck, E. F., Lahuis, F., et al. 2003, A&A, 399, 1047
Bottger, G. L., & Eggers, D. F., Jr 1964, JChPh, 40, 2010
Boudin, N., Schutte, W. A., & Greenberg, J. M. 1998, A&A, 331, 749
Bouilloud, M., Fray, N., Benilan, Y., et al. 2015, MNRAS, 451, 2145
Brock, A., Mina-Camilde, N., & Manzanares, C. 1994, JPhCh, 98, 4800
Burkhardt, A. M., Long Kelvin Lee, K., Bryan Changala, P., et al. 2021, ApJL, 913, L18
Cabezas, C., Agúndez, M., Pérez, C., et al. 2025, A&A, 701, L8
Cao, L., Mühlberger, F., Adam, T., et al. 2003, AnaCh, 75, 5639
Carr, J. S., & Najita, J. R. 2008, Sci, 319, 1504
Cernicharo, J., Agúndez, M., Cabezas, C., et al. 2021, A&A, 649, L15
Cernicharo, J., Heras, A. M., Tielens, A. G. G. M., et al. 2001, ApJ, 546, L123
Comeford, J. J., & Gould, J. H. 1961, JMoSp, 5, 474
Derenne, S., & Robert, F. 2010, M&PS, 45, 1461

Dey, D., Woodhouse, J. L., Taylor, M. P., Fielding, H. H., & Worth, G. A. 2024, PCCP, 26, 3451
D'Hendecourt, L. B., & Allamandola, L. J. 1986, A&AS, 64, 453
Doney, K. D., Zhao, D., Stanton, J. F., & Linnartz, H. 2018, PCCP, 20, 5501
Drouin, D., Couture, A. R., Joly, D., et al. 2007, Scanning, 29, 92
Dyke, J. M., Ozeki, H., Takahashi, M., Cockett, M. C. R., & Kimura, K. 1992, JChPh, 97, 8926
Ehrenfreund, P., & Cami, J. 2010, CSHPB, 2, a002097
Fendt, A., Geissler, R., Streibel, T., Sklorz, M., & Zimmermann, R. 2013, TcAc, 551, 155
Ferrari, B. C., Slavicinska, K., & Bennett, C. J. 2021, AcChR, 54, 1067
Ghosh, R., Sil, M., Kumar Mondal, S., et al. 2022, RAA, 22, 065021
Goettl, S. J., Ahmed, M., Mebel, A. M., & Kaiser, R. I. 2025, AcChR, 58, 2682
Goettl, S. J., Yang, Z., He, C., et al. 2024, FaDi, 251, 509
Hagen, W., Tielens, A. G. G. M., & Greenberg, J. M. 1981, CP, 56, 367
Heger, H. J., Zimmermann, R., Dorfner, R., et al. 1999, AnaCh, 71, 46
Herd, C. D. K., Blinova, A., Simkus, D. N., et al. 2011, Sci, 332, 1304
Hertz-Schünemann, R., Dorfner, R., Yeretzian, C., Streibel, T., & Zimmermann, R. 2013, JMSp, 48, 1253
Holstein, W. L., Hammer, M. R., Metha, G. F., & Buntine, M. A. 2001, IJMSp, 207, 1
Hudgins, D. M., Sandford, S. A., Allamandola, L. J., & Tielens, A. G. 1993, ApJS, 86, 713
Hudson, R. L., Ferrante, R. F., & Moore, M. H. 2014, Icar, 228, 276
Jiang, G. J., Person, W. B., & Brown, K. G. 1975, JChPh, 62, 1201
Jones, B. M., & Kaiser, R. I. 2013, JPCL, 4, 1965
Kaiser, R., & Roessler, K. 1997, ApJ, 475, 144
Kaiser, R. I., Maity, S., & Jones, B. M. 2014, PCCP, 16, 3399
Kaiser, R. I., Parker, D. S. N., & Mebel, A. M. 2015, ARPC, 66, 43
Kaiser, R. I., & Roessler, K. 1998, ApJ, 503, 959
Kaiser, R. I., Zhao, L., Lu, W., et al. 2022, JPCL, 13, 208
Kim, Y. S., & Kaiser, R. I. 2009, ApJS, 181, 543
Kleimeier, N. F., & Kaiser, R. I. 2022, JPCL, 13, 229
Kleimeier, N. F., Liu, Y., Turner, A. M., et al. 2022, PCCP, 24, 1424
Kolesniková, L., Daly, A. M., Alonso, J. L., Tercero, B., & Cernicharo, J. 2013, JMoSp, 289, 13
Koops, T., Visser, T., & Smit, W. M. A. 1984, JMoSp, 125, 179
Lacy, J. H., Evans, N. J., , I. I., et al. 1989, ApJ, 342, L43
Lahuis, F., & van Dishoeck, E. F. 2000, A&A, 355, 699
Lara, L. M., Lellouch, E., López-Moreno, J. J., & Rodrigo, R. 1996, JGR, 101, 23261
Linstrom, P. J., & Mallard, W. G. 2013, NIST Standard Reference Database Number 69, NIST Chemistry webBook, http://webbook.nist.gov/ (accessed 2025-11-14)
Maity, S., Kaiser, R. I., & Jones, B. M. 2014, ApJ, 789, 36
McGuire, B. A., Burkhardt, A. M., Kalenskii, S., et al. 2018, Sci, 359, 202
McMullan, R. K., Kvick, A., & Popelier, P. 1992, AcCrB, 48, 726
Menor-Salván, C., Ruiz-Bermejo, M., Osuna-Esteban, S., Muñoz-Caro, G., & Veintemillas-Verdaguer, S. 2008, Chem Biodivers, 5, 2729
Mojarro, A., Buch, A., Dworkin, J. P., et al. 2023, JGRE, 128, e2023JE007968
Mumma, M. J., DiSanti, M. A., Dello Russo, N., et al. 2003, AdSpR, 31, 2563
Nix, M. G. D., Devine, A. L., Cronin, B., Dixon, R. N., & Ashfold, M. N. R. 2006, JChPh, 125, 133318
Nna-Mvondo, D., & Anderson, C. M. 2022, ApJ, 925, 123
Öberg, K. I., Boogert, A. A., Pontoppidan, K. M., et al. 2011, ApJ, 740, 109
Parker, J. K., & Davis, S. R. 1999, JAChS, 121, 4271
Piacentino, E. L., Balkanski, A., Rajappan, M., & Öberg, K. I. 2024, ApJ, 974, 313
Ratzer, C., Küpper, J., Spangenberg, D., & Schmitt, M. 2002, CP, 283, 153
Ridgway, S. T., Hall, D. N. B., Wojslaw, R. S., Kleinmann, S. G., & Weinberger, D. A. 1976, Natur, 264, 345
Rivilla, V. M., Jiménez-Serra, I., Martín-Pintado, J., et al. 2021, PNAS, 118, e2101314118
Robertson, C., Hyland, R., Lacey, A. J. D., Havens, S., & Habershon, S. 2021, JCTC, 17, 2307
Ruscic, B., & Bross, H. 2025, in Active Thermochemical Tables (ATcT) values based on ver. 1.220 of the Thermochemical Network (Argonne National Laboratory) https://atct.anl.gov/Thermochemical%20Data/version%201.220/index.php
Sephton, M. A., Chan, Q. H. S., Watson, J. S., et al. 2024, M&PS, 59, 1131
Seta, T., Nakajima, M., & Miyoshi, A. 2006, JPCA, 110, 5081
Thomas, A. M., Doddipatla, S., Kaiser, R. I., Galimova, G. R., & Mebel, A. M. 2019, NatSR, 9, 17595
Tielens, A. G. G. M. 2013, RvMP, 85, 1021
Tsuge, M., Kouchi, A., & Watanabe, N. 2022, ApJ, 933, 138
Turner, A. M., Abplanalp, M. J., Chen, S. Y., et al. 2015, PCCP, 17, 27281
Turner, A. M., & Kaiser, R. I. 2020, AcChR, 53, 2791
Turner, A. M., Koutsogiannis, A. S., Kleimeier, N. F., et al. 2020, ApJ, 896, 88
Tørneng, E., Nielsen, C. J., Klaeboe, P., Hopf, H., & Priebe, H. 1980, AcSpA, 36, 975
Wang, J., Marks, J. H., Turner, A. M., et al. 2023, PCCP, 25, 936
Wang, J., Nikolayev, A. A., Marks, J. H., et al. 2024a, JAChS, 146, 28437
Wang, J., Zhang, C., Marks, J. H., et al. 2024b, NatCo, 15, 10189
Watson, J. S., Sephton, M. A., & Gilmour, I. 2010, IJAsB, 9, 201
Wenzel, G., Gong, S., Xue, C., et al. 2025, ApJL, 984, L36
Woon, D. E., & Park, J.-Y. 2004, ApJ, 607, 342
Xie, C., Ma, J., Zhu, X., et al. 2016, JAChS, 138, 7828
Yeghikyan, A. G. 2011, Ap, 54, 87
Zeichner, S. S., Aponte, J. C., Bhattacharjee, S., et al. 2023, Sci, 382, 1411
Zeng, S., Jiménez-Serra, I., Rivilla, V. M., et al. 2021, ApJ, 920, L27
Zhang, C., Zhu, C., Turner, A. M., et al. 2023, SciA, 9, eadg6936
Zheng, W., Jewitt, D., & Kaiser, R. I. 2006, ApJ, 639, 534
Zhou, L., Zheng, W., Kaiser, R. I., et al. 2010, ApJ, 718, 1243